



Cite this: *RSC Appl. Polym.*, 2025, **3**, 1325

# Concentric half-domain spacing morphologies and anomalous domain stretching in microwave annealed block copolymer thin films†

Ugur Aslan,<sup>a</sup> Maninderjeet Singh,<sup>b</sup> Akhtar Gul,<sup>a</sup> Jack F. Douglas <sup>c</sup> and Alamgir Karim <sup>\*b</sup>

Block copolymer (BCP) films hold significant promise for a wide array of technological applications, including nanopatterning, nanophotonics, polymer electrolytes, and optical waveguides. However, the practical realization of these applications is often hindered by the slow kinetics of the ordering of block copolymers, attributed to the inherently glassy dynamics of polymeric soft materials under standard processing conditions. The diverse range of BCP morphologies further highlights the unique self-assembly characteristics of polymeric materials. In this study, we employ a microwave annealing method that generates a high substrate heating rate ( $18\text{ }^{\circ}\text{C s}^{-1}$ ) to rapidly order lamellar BCP thin films on a high-resistivity boron-doped silicon substrate. This substrate efficiently absorbs microwave energy, creating a rapid and substantial  $z$ -temperature gradient in the BCP film. The high-temperature annealing facilitated by microwave heating generates  $1L_0$  surface terraces composed of unconventional rim-like morphologies with a  $0.5L_0$  (half domain spacing) height, forming half-domain height island-on-island and hole-in-hole topographies. We hypothesize that these topographies are related to the highly dynamic through-film thickness temperature gradient. Notably, reducing the substrate heating rate to  $13.5\text{ }^{\circ}\text{C s}^{-1}$  only produces interesting  $0.5L_0$  top surface structures. Additionally, the elevated high temperatures of microwave annealing significantly increase the vertical lamellar domain size,  $L_0$ , of the BCP film surface topography, which we believe corresponds to an “intermediate segregation” regime of chain stretching. This domain size enhancement is due to the synergy of the reduced interaction parameter between blocks and improved interlayer diffusional dynamics resulting from the sharp temperature spike and rapid vitrification. These unique morphological effects, exclusive to microwave annealing, are not seen in conventional thermal or solvent annealing and open new avenues for microwave substrate-directed self-assembly (MS-DSA) to create unique surface and internal BCP morphologies for specialized applications.

Received 22nd April 2025,  
Accepted 20th July 2025

DOI: 10.1039/d5lp00116a

rsc.li/rscapppolym

## 1. Introduction

It is well-known that diblock copolymers self-assemble into periodic well-defined and unique nanostructures under equilibrium conditions, with morphologies such as lamellae, cylinders, spheres, gyroids, *etc.*, depending on the relative molar mass volume ratio of the blocks and interaction parameter,  $\chi_{AB}$ . Thin films can exhibit a high sensitivity to processing conditions under which self-assembly and ordering occur, as is the case with polymer crystallinity.<sup>1</sup> As-cast thin films of block

copolymers (BCPs) often remain in a vitrified, disordered, and nonequilibrium state after being cast from solutions in neutral or good solvents.<sup>2–5</sup> The BCP films typically require post-processing steps, known as “annealing”, to increase the mobility of BCP chains, enough to allow them to organize into morphologies closer to their thermodynamic equilibrium state.<sup>6</sup> Conventional annealing methods primarily involve thermal annealing<sup>7–10</sup> and exposure to solvent immersion or solvent vapor annealing.<sup>11,12,83</sup> Some additional enhancements include applied electric field,<sup>13</sup> shearing the films,<sup>14,15</sup> subjecting them to transient heating “cold-zone annealing”,<sup>16</sup> laser-induced annealing,<sup>17</sup> mixed-solvent vapor annealing,<sup>18</sup> solvothermal annealing,<sup>19</sup> sequential annealing<sup>8,20</sup> and microwave annealing.<sup>21,22</sup> Nonetheless, the slow kinetics, often complex and costly experimental design, and limited applicability remain as general challenges in developing the full potential of BCP films for cutting-edge nano-technological applications such as nanolithography,<sup>23</sup> fuel cells,<sup>24,25</sup> nanofiltration

<sup>a</sup>Materials Science and Engineering, University of Houston, TX 77004, USA<sup>b</sup>William A. Brookshire Department of Chemical and Biomolecular Engineering, University of Houston, TX 77004, USA. E-mail: akarim3@central.uh.edu<sup>c</sup>Materials Science and Engineering Division, National Institute of Standards and Technology, Gaithersburg, MD 20899, USA† Electronic supplementary information (ESI) available. See DOI: <https://doi.org/10.1039/d5lp00116a>

membranes,<sup>26,27</sup> photonics,<sup>28</sup> and dielectric polymeric capacitors.<sup>29</sup> At present, traditional thermal annealing remains the most widely used and scientifically important method for creating stable nanostructures in BCP thin films, even though alternate annealing methods have shown that other morphologies of great potential interest can be created by annealing the BCP films under non-equilibrium conditions.

The lamellar morphology of BCP thin films forms due to the existence of air and substrate boundaries of the films, which have a preferential affinity for the blocks. Lamella-forming BCPs traditionally create islands or holes with the dimension (height perpendicular to the plane of the film) of an equilibrium domain spacing,  $L_0$ , that is inherently determined by the average BCP molecular mass,  $M_n$ . Less studied is how the domain spacing of the thin films may also be varied by quenching the BCP films into non-equilibrium states depending on the processing method used, *e.g.*, solvent vapor annealing (SVA), direct immersion annealing (DIA), *etc.* These island and hole formations in BCP thin films under equilibrium conditions are a consequence of incommensuration of film thickness as a multiple of the domain spacing, *i.e.* islands and holes form on the film surface of quantized depth equal to one domain spacing,  $1L_0$ , if the thickness ( $h$ ) of the BCP thin film is not equal to an integer ( $n$ ) multiple of the domain spacing,  $L_0$ , *i.e.*  $h_0 = nL_0$  for symmetric wetting of the air and substrate interfaces by the same one block and  $(h_0 = (n + 0.5)L_0$  for an asymmetric wetting which has different polymer blocks wetting at the substrate and air interface).<sup>30,31</sup> The lamellar domain thickness,  $L_0$ , is comprised of layers of A-*b*-B : B-*b*-A, where *b* refers to block, where A and B are the block polymer components, commonly referred to as “ABBA” layered domains.

Understanding the formation of these island and hole surface structures is paramount to clearly understanding the interfacial interactions of polymer chains with the processing environment and predicting the kinetics of ordering lamellar BCP thin films by chiefly studying the film topography. Notably, a single BCP sublayer in the typical domain thickness of  $L_0$  contributes  $0.5L_0$  height, *i.e.*, the AB of the ABBA domain. For asymmetrical wetting, driven by selective attractive interaction of a block with the substrate and lower surface tension of the other block at the air interface typically, in thin BCP films, islands form when the thickness,  $h_0$ , is between  $(n + 0.5)L_0 < h_0 < (n + 1)L_0$ , and holes form once the thickness is between  $(nL_0) < h_0 < (n + 0.5)L_0$  and *vice versa* for symmetric BCP thin films.<sup>32–35</sup> Film topography transitions from surface  $1L_0$  height holes when the film thickness just exceeds the nearest commensurability criteria to progressively exhibit a narrow bi-continuous window also of  $1L_0$  height structures, to  $1L_0$  height islands as the film thickness approaches the next  $n$  value of commensurate thickness.<sup>30,36</sup> The “traditional” thermal annealing method for BCP ordering suffers from long annealing times, often ranging from hours to days, and requires high-temperature processing, above glass transition temperatures of the component blocks of BCPs, making this processing method unattractive. In this regard, microwave

annealing can alleviate the drawbacks of thermal annealing. Microwave heating is widely used as an alternative to conventional thermal heating in various fields, including the food industry,<sup>37</sup> organic synthesis,<sup>38</sup> and catalysis<sup>39</sup> due to its advantages of rapid heating, economic feasibility, high-yield, and high-purity outcomes.<sup>40</sup> This method involves the absorption of electromagnetic radiation within the frequency range of 300 MHz to 300 GHz, situated between infrared and radio frequencies. The first reported use of microwaves in chemistry dates back to the 1970s.<sup>41</sup> Microwave energy absorption excites the vibrational and rotational modes of molecules in the material, which is then converted into thermal motion as the excited species relax through intermolecular collisions and other phonon modes of energy transfer.<sup>38</sup> Compared to traditional thermal heating procedures, microwave heating offers benefits such as volumetric and selective heating, and faster processing times. However, it is a complex process that requires careful implementation due to the potential for destructive and constructive interference of electromagnetic radiation, which can create hot and cold spots and result in non-uniform heat distribution within the material.<sup>42</sup>

Several studies have explored microwave annealing as a versatile method for ordering various BCP structures.<sup>21,43–47</sup> Pioneering work by Buriak and colleagues investigated BCP film ordering using both a microwave oven and a microwave reactor. They demonstrated perpendicular ordering of BCPs on silicon substrates, both with and without the presence of a solvent.<sup>21,22</sup> For solvent-free microwave annealing, Buriak's team used BCP films sandwiched between a microwave-neutral substrate and a microwave-absorbing silicon wafer, which heated the BCP films and resulted in fast ordered structures.<sup>22</sup> This work established the importance of the substrate's microwave absorption properties in the annealing process. Morris and colleagues later showed that cylinder-forming BCP thin films could be ordered using a microwave reactor with a neutral brush grafted on the silicon wafer, concluding that graphoepitaxy and microwave annealing are compatible.<sup>48</sup> Vogt and coworkers further highlighted the significance of the position and orientation of the target material, in this case, thin films, within the commercial microwave chamber, as well as the properties of the microwave energy, to achieve ordered cylindrical BCP films.<sup>49</sup> Although previous studies have not addressed the scalability of this method, microwave annealing of BCP thin films appears to be a rapid, reliable, and cost-effective processing technique. In principle, BCP films should achieve similar results with microwave annealing in seconds, compared to days with conventional annealing methods. However, the unique effects arising from the rapid thermal gradient produced during microwave interaction have not been previously reported, which we address in this article. Notably, all prior microwave annealing studies have focused on pattern formation using either cylinder-forming BCPs or vertical lamellae. In contrast, this study examines microwave-assisted parallel ordering of lamellar BCPs, their surface morphology, and the associated dynamics, which have not been previously explored.



In this study, we investigate the lamellar ordering of BCP thin films through microwave annealing at short annealing times, ranging from 5 seconds (s) to 15 seconds. We demonstrate how the duration of microwave annealing affects the ordering of BCP thin films, resulting in unique surface topographies. Numerous studies have detailed the surface morphology formation of lamellar BCP films,<sup>50–55</sup> with notable pioneering work by Russell *et al.*<sup>35,56</sup> Regarding the kinetics of BCP surface topography evolution into islands and holes, Smith *et al.* meticulously examined terrace formations in films with a continuous thickness gradient, allowing simultaneous study of regions with varying degrees of thickness incommensurability. They observed the formation of equilibrium islands and holes with heights equivalent to the domain size ( $L_0$ ) in relation to thermal annealing time and temperature, up to 170 °C.<sup>31</sup> For instance, the average surface hole diameter of parallel lamella-forming polystyrene-*block*-poly(methyl methacrylate) (PS-*b*-PMMA) (25 000)–(26 000) g mol<sup>−1</sup>, labeled as (*Lml*<sub>51</sub>), increased up to 3 μm over 48 h and remained stable up to 100 h of thermal annealing. In contrast, microwave heating typically induces localized heating spots on the substrate, potentially creating different surface morphologies in a spatially heterogeneous manner, depending on the in-plane thermal conductivity of the substrate (see ESI S1†). High thermal conductivity substrates, such as silicon wafers, can rapidly homogenize heating from these non-uniformly distributed hot spots. This is the case for our microwave-absorbing high-resistivity silicon wafer doped with boron (B-doped Si), among other silicon substrates. Consequently, our B-doped Si substrates induce a rapid but relatively homogeneous in-plane temperature distribution across the substrate. The novelty of the morphological BCP features reported here is primarily due to the rapid heating profile between the non-microwave-absorbing BCP film and the microwave-absorbing substrate.

Complex droplet liquid surfaces after a long oven annealing time, 100 h, at 180 °C, such as block copolymers in the melt state, transitioning from an isotropic disordered state to an anisotropic ordered state, can be stacked in concentric step-layered morphology.<sup>57</sup> Our study reveals that the BCP film morphology obtained through microwave annealing includes symmetric island-on-island and hole-in-hole structures, features not observed in traditional oven or solvent annealing processes. These ordered parallel lamellar structures form within seconds, exhibiting  $0.5L_0$  height and multiple concentric boundaries (see the TOC figure). Previous studies by Willson *et al.* have reported regular (non-concentric)  $0.5L_0$  island/hole formations using block copolymer films, such as poly(styrene-*block*-4-trimethylsilylstyrene) (PS-*b*-PTMSS)<sup>58</sup>, and partially epoxidized poly(styrene-*block*-isoprene) (PS-*b*-PEI78)<sup>34</sup> diblock copolymers, which were manipulated to have one neutral interface, air or substrate. Willson *et al.* observed the  $0.5L_0$  height islands or holes during the intermediate stages of developing  $1L_0$  height islands or holes through thermal annealing of lamellar BCPs.<sup>58</sup> However, concentric  $0.5L_0$  surface morphologies with well-developed lamellar structures have not been produced by other annealing methods to our knowledge.

The average diameter of the hole-in-hole structures increased with microwave annealing time, evolving towards spinodal-like island formation at the same as-cast thickness. In contrast, traditional  $1L_0$  holes transition to spinodal formations due to thickness increments of BCP films during classic thermal oven annealing.<sup>30</sup> The average diameter of hole-in-hole structures reached approximately 3 μm in 10 s and continued to increase until spinodal-like or island-like morphologies formed in 15 s.

We also report the time evolution of enhanced lamellar domain spacing ( $L_0$ ) with microwave annealing time, showing an unusually high trend in  $L_0$  increment with microwave annealing temperature, suggesting unusual chain stretching and packing dynamics under rapidly evolving non-equilibrium conditions, which are quenched upon cooling into a glassy state. The strong segregation limit (SSL) theory predicts domain spacing,  $L_0 \approx bN^{2/3}\chi^{1/6}$ , which gives a weak temperature dependence assuming  $\chi \sim 1/T$ , a predicted trend cannot explain our results.<sup>59</sup> This increment also exceeds predictions based on the coefficient of thermal expansion (CTE) for the temperature change induced by microwave annealing.<sup>60</sup> Notably, such anomalous domain stretching has scant literature context except for SAXS studies by Baldrian *et al.*<sup>61</sup> in a 100 mm thick (bulk) PS(40k)-*b*-PMMA(40k) film, in the temperature range of 150–200 °C, wherein domain spacing essentially doubled from 26 nm to 52 nm. This high expansion was not observed in their lower  $M_w$  PS(4.8k)-*b*-PMMA(6k). They hypothesized that a temperature-dependent transition from strong to an “apparent” weak segregation limit (WSL) could arise in reasonable correspondence with their data. In summary, we have investigated the variations in surface morphology and domain spacing of microwave-ordered parallel lamellar BCP thin films, considering the different block types, molecular mass, film thickness, and processing time.

## 2. Experimental section

### Microwave oven and block copolymers

The microwave oven's dimensions were 25 cm × 30 cm × 30 cm, covering a volume of approximately 15 liters. A rotating plate was at the bottom center of the microwave oven to distribute the microwave exposure uniformly over the substrate. The PS-*b*-PMMA block copolymer has an number average molecular mass  $M_n$  = PS (25 000)-*b*-PMMA (26 000) g mol<sup>−1</sup> with polydispersity index, PDI, of 1.06,  $M_n$  = PS (19 500)-PMMA (17 000) g mol<sup>−1</sup> with PDI of 1.05, and poly(styrene)-*b*-poly(2-vinyl pyridine) (PS-*b*-P2VP) with a molecular mass,  $M_n$ , of PS (25 000)-*b*-P2VP(25 000) g mol<sup>−1</sup> with PDI of 1.06. All BCP relative volume fractions correspond to the lamellar morphology ( $f_A \approx 0.5$ ) and were purchased from Polymer Source Inc. Lamellar forming block PS-*b*-PMMA copolymers are represented with the abbreviation of *Lml*<sub>*m*</sub> where subscript *m* is the total molecular mass in kg mol<sup>−1</sup>, for *e.g.*, PS (25 000)-*b*-PMMA (26 000) g mol<sup>−1</sup> is represented as *Lml*<sub>51</sub>. The polymer solutions were prepared with a mass fraction of 2% relative to the solvent, anhydrous toluene, having 99.8% purity. 2 mass%



of PS-*b*-PMMA in toluene was mixed for 24 hours. The polymer was completely dissolved to obtain a clear solution and filtered using a microfilter with 40  $\mu\text{m}$  pores to remove the contaminants. Thin BCP films were prepared by flow coating. Flow coating requires minute quantities of polymer solution, which was pipetted into a capillary-sized (less than 1 mm) gap between an angled glass blade and the flat silicon substrate. The glass blade moved along the substrate, pulling the bulk of the solution while leaving a thin layer that dried to form a solid film. The thin film thicknesses ranged from 30 nm to 130 nm. The solid thin films were then placed inside a conventional oven for 24 h at 50  $^{\circ}\text{C}$  to evaporate any residual solvent. The thicknesses of the BCP thin films were measured using an interferometer, FILMETRICS LS-DT2.

### Substrates

Boron-doped (B-doped) silicon (Si) wafers (P-type) having a resistivity of (1–100)  $\Omega\text{ cm}$  ( $P_{\text{H}}$ ) (High resistivity) referred as *P-type2*, (0.008–0.01)  $\Omega\text{ cm}$  ( $P_{\text{L}}$ ) (Low resistivity) referred as *P-type* and antimony (Sb) doped silicon wafers (N-type) having a resistivity of (0.01–0.02)  $\Omega\text{ cm}$  ( $N_{\text{L}}$ ) (Low resistivity) referred as *N-type* were used as substrates. They were purchased from UniversityWafer. The thickness of the boron-doped silicon wafer was 1055  $\mu\text{m}$  to 1075  $\mu\text{m}$  with a precision of 25  $\mu\text{m}$ . The silicon wafer was cut to have a dimension of approximately 15 cm by 10 cm with three straight edges and one rounded edge (due to the original wafer's disk-like shape). The cut B-doped silicon wafers were treated using an ultraviolet–ozone (UVO) chamber and irradiated with ultraviolet (UV) light of 184.9 nm and 253.7 nm wavelengths for two hours to remove organic impurities and oxidize the surface. Microwave annealing was done using a laboratory-grade microwave oven, MTST, with a maximum power of 650 watts. BCP thin films are highly sensitive to the air, which can degrade the films before they are ordered. So, we used an in-house ceramic vacuum chamber. The vacuum chamber was placed inside the microwave oven with the BCP thin film sample. The position of the vacuum chamber with respect to the microwave stage was fixed to ensure consistent exposure. The samples were removed immediately after the desired annealing time and cooled to room temperature by placing the wafers on an aluminum block. The BCP constituents did not significantly heat up by microwave treatment but absorbed heat directly from the microwave-absorbing substrate.

### Film characterization

The BCP thin films were investigated by Atomic Force Microscopy (AFM) using a Bruker AXS-Dimension Icon. The AFM tapping mode was used to obtain the surface morphologies of the BCP thin films. The height and phase images were processed using Bruker NanoScope software to remove noise and artifacts.

### Temperature measurement

The measurements were performed for the same sample sizes, repeated three times, and averaged. The temperatures of the

BCP thin films were measured with an infrared thermometer (IR) as soon as the microwave irradiation was completed by immediately opening the microwave oven's door. Our reported temperature should be considered as the BCP film temperature based on the BCP film. This is because the B-doped Si wafers showed almost the same temperature for a given time without a BCP film on top. After all, the IR emissivity from the hot base B-doped Si wafer is minimally absorbed by the BCP film, given that the film thicknesses are well below 100 nm used in the study.

On the other hand, the transient temperature gradient  $d(\text{DT}/h)/dt$  normal direction to the film thickness ( $h$ ) direction in the rapidly heating BCP film can be large because of the synergy of the low thermal conductivity of polymers in conjunction with the small value of film thickness  $h$  in the denominator. However, very advanced metrology would be required to measure this transient temperature gradient, especially given the constraints of the microwave geometry. Even with a millisecond (ms) response GaAs fiber optic temperature sensor or even a regular thermocouple that can in fact be inserted through a top microwave port, the problem is that any reliable physical contact with the force of the sensor on top of a 45 nm polymer film will compromise the film thickness locally, especially when heated from its glassy to a melt state well above  $T_{\text{g}}$  such as encountered in microwave annealing. Thus, it will not be an accurate measure of the BCP film top surface temperature. Action at a distance dielectric fiber optic temperature sensor may work, but we did not have the resources for obtaining such a setup, and these will need extensive temperature calibration as well. Future work with collaborators will aim to develop this worth-while transient temperature gradient capability in the through-film thickness ( $z$  or  $h$ ) direction.

## 3. Results and analyses

### Formation of concentric islands and holes

Traditional thermal oven annealing (TA) was used to order lamellae forming 25k–26k PS-*b*-PMMA BCP thin films at 230  $^{\circ}\text{C}$  for 24 h in a high vacuum, as a means to produce control samples with uniform isotropic heating, and compared subsequently to microwave annealed samples, wherein the B-doped Si substrate is the only rapid heating element producing a large thermal gradient in the film thickness direction from the substrate to air (presented later). Asymmetric wetting PS-*b*-PMMA TA films produced islands with a height of 35 nm ( $L_0$  –37.5 nm estimated for the melt state at the annealing temperature with the coefficient of thermal expansion (CTE) correction) as shown in Fig. 1a. Recalling that holes on the incommensurate BCP thin films form once the film thickness  $h_0$  is between  $(nL_0) < h_0 < (n + 0.5)L_0$ , with integral values of  $n$ , with experimentally determined  $L_0 = 37.5\text{ nm}$ , holes formed once the as-cast film thickness, was adjusted to  $h_0 = 45\text{ nm} = 1.20L_0$  ( $1L_0 < 1.20L_0 < 1.5L_0$ ),  $h_0 = 55\text{ nm} = 1.36L_0$  ( $1L_0 < 1.46L_0 \sim 1.5L_0$ ), and  $h_0 = 120\text{ nm} = 3.20L_0$  ( $3L_0 < 3.20L_0 < 3.5L_0$ ), as





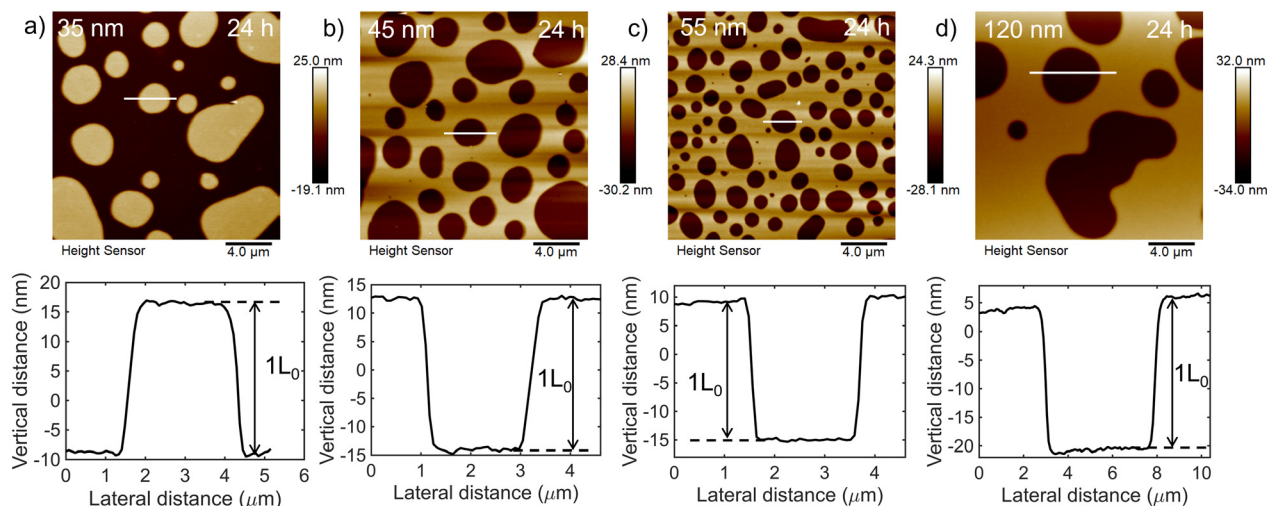


**Fig. 1** Thermal annealing of PS-*b*-PMMA thin films in traditional ovens at 230 °C for 24 h: (a) 35 nm, (b) 45 nm, (c) 55 nm and (d) 120 nm thicknesses.

shown in Fig. 1b, c, and d, respectively. The line profiles are drawn across the islands and holes of each AFM image to determine the domain spacing ( $L_0$ ) of each film. All films showed fully grown  $1L_0$  height as either islands or holes as expected after annealing for 24 h at 230 °C. These confined islands and holes are consistent with the incommensurability for the preferential affinities of the PS and PMMA blocks segregating at the interfaces as evidence of parallel-lamellar morphologies. These traditional island and hole morphologies span throughout the film surface as a single layer of either island or hole. Thin films of PS-*b*-PMMA (25 K–26 K),  $L_{ml51}$ , PS-*b*-PMMA (19.5 K–17 K),  $L_{ml36.5}$ , and PS-*b*-P2VP (25 K–25 K),  $L_{ml50}$ , were processed by microwave heating, and the temperatures of the high-resistivity B-doped Si substrate were recorded as a function of time (5 s, 8 s, 10 s, 12 s, 15 s, and 20 s).

The microwave electromagnetic energy (electromagnetic energy operating in the frequency at 2.45 GHz) coupling with the *P-type2* substrate making its temperature rise significantly in a short time (no significant amount of microwave energy was absorbed directly by the PS-*b*-PMMA polymer film, as tested on the non-absorbing substrate), imparting mobility to the polymer chains, which resulted in their parallel lamellar ordering due to the preferential migration of the PMMA blocks to the SiO<sub>x</sub> layer on the substrate and PS blocks to the air interface.

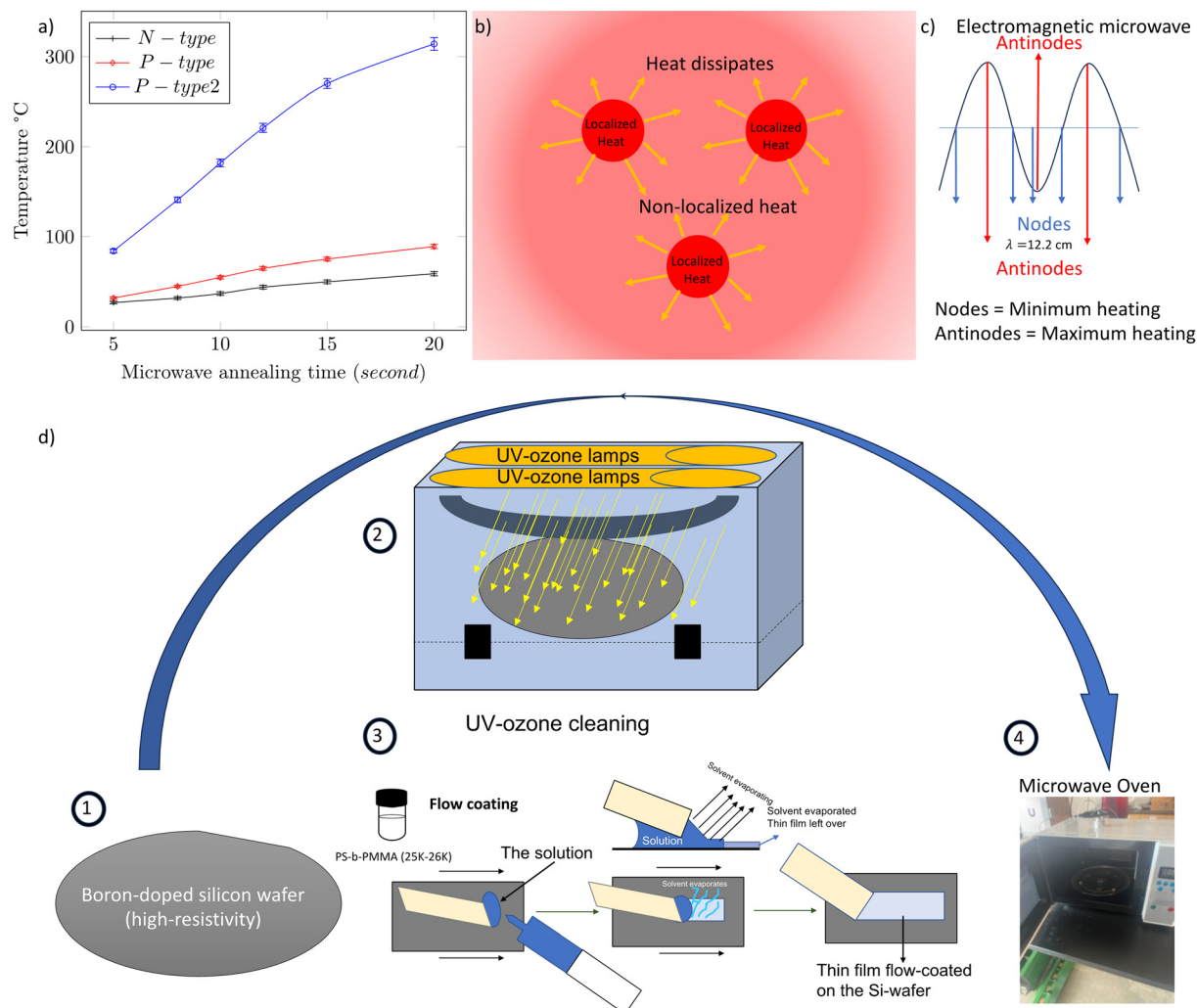
As in thermally annealed films under near-equilibrium conditions, incommensurate film thicknesses produced a surface morphology of islands and holes. The temperature  $T_s$  of the substrate, *P-type2*, in the microwave was found to be 85 °C at 5 s and as high as 320 °C at 20 s, indicating very high heating rates, much faster than traditional vacuum thermal ovens where heating occurs mostly by conduction. The hole growth of BCP thin films is recorded for only up to 15 s with a substrate temperature of 270 °C (the films de-wet after about 20 s due to the substrate temperature reaching 320 °C, as shown in

Fig. 2a, which we are also concerned about eventual polymer degradation). The exposure time of microwave annealing on BCP thin films is critical due to the rapid high-temperature increment, which changes their block-block thermodynamic interactions in addition to providing mobility. Microwave heating differs from traditional thermal annealing, due to the dynamic and rapid increase in temperature, for instance, 15 °C per second, while for traditional thermal annealing, the temperature increases slowly.<sup>62</sup> The *P-type2* substrate heats up extremely rapidly under microwave irradiation, with the temperature reaching and surpassing the glass transition temperatures of PS, 100 °C, and PMMA, 115 °C, blocks within 8 s of irradiation.

The short-time ultrafast dynamics of microwave-heated BCP thin films produces a novel surface feature of a  $0.5L_0$ -step height of islands or holes, surrounded by another layer step of  $0.5L_0$  height islands or holes (the hole-in-hole morphology is shown in Fig. 3) with concentric boundaries, which we refer to as hole-in-hole and island-on-island morphologies. Since  $1L_0$  is the domain spacing corresponding to ABBA,  $0.5L_0$  or half-step height corresponds to only AB (*i.e.*, single diblock, *e.g.*, PS-*b*-PMMA) layer thickness. The hole-in-hole feature has a symmetric step surrounding the first hole with a very small step width (in-plane of the film) before the boundary of the second hole.

The AFM height image of Fig. 3a with a vibrant brown color scale strikingly indicates the height differences and step widths. The khaki brown rings around the chocolate brown holes indicate the  $0.5L_0$ -step holes (magnified in Fig. 3c). The AFM phase images show that the surface of the hole-in-hole and the bottom of the hole-in-hole morphology (domain thickness,  $L_0$ ) have the same phase shift, indicating that the same polymer is present at the bottom and surface of the hole-in-hole of the film (Fig. 3b). The phase shift,  $\lambda$ , from the line profile of the AFM phase image in Fig. 3d shows a difference





**Fig. 2** (a) Microwave heating response of silicon wafers, *P*-type (low-resistivity), *N*-type (low-resistivity), and *P*-type2 (high-resistivity), are recorded up to 20 seconds (b) The schematic of the hypothetical heating response of the silicon wafer under microwave radiation, (c) the schematic of electromagnetic microwave radiation which heats the substrate highest at antinodes, and lowest at nodes (d) the schematic of the block copolymer thin film's experimental procedure starting with the B-doped Si wafer ( $\approx 15$  cm  $\times$  10 cm) (1), undergoing UVO exposure (2), flow coating of the polymeric BCP solution as a thin film on the substrate (3), and the the sample is placed into the microwave oven (4).

between the  $0.5L_0$  step height and other places, which are the surface and bottom of the  $1L_0$  hole. The hole and the surface representing the PS have similar AFM phase angles (no phase-shift), whereas the  $0.5L_0$ -step height indicates that the PMMA, which has a phase shift, not to be confused with the two long and sharp crests, which come from edge effects, an artifact of scanning, which is shown in Fig. 3d. The magnified hole from the AFM height image indicates the line profile drawn over the edge of the hole-in-hole to show the relative heights, as presented in Fig. 3c.

Fig. 4 shows the change of the lamellar periodicity in the thin film starting at 5 s, continuing to 8 s, 10 s, 12 s, and 15 s, resulting in higher temperatures quantified as 85 °C, 141 °C, 182 °C, 221 °C, and 270 °C, respectively. As the substrate heats up and the temperature reaches above the glass transition temperature,  $T_g$ , of the blocks, the PMMA block selectively

diffuses toward the  $\text{SiO}_2$  layer. On the other hand, the PS block with a lower surface energy segregates onto the air-film interface. The 5 s microwave annealing of the BCP thin film does not show any surface morphology due to insufficient substrate heating by microwave energy and the temperature remains below the glass transition temperature of BCP films. This surface structure indicates that the BCP thin film is not yet in a fully ordered state throughout the film thickness as fully through-thickness ordered incommensurate BCP films should produce islands or holes upon parallel-lamellar ordering. As the microwave annealing time is extended, the thin film exhibits a parallel lamellar morphology, as shown in Fig. 4a and b at 8 s of annealing. The total hole height (adding heights for both, barely visible, steps) on the surface of the thin film is equal to the period of the lamellar structure,  $1L_0$ .<sup>63</sup> As the microwave exposure time increases to 10 s and 12 s, the concentric rims at



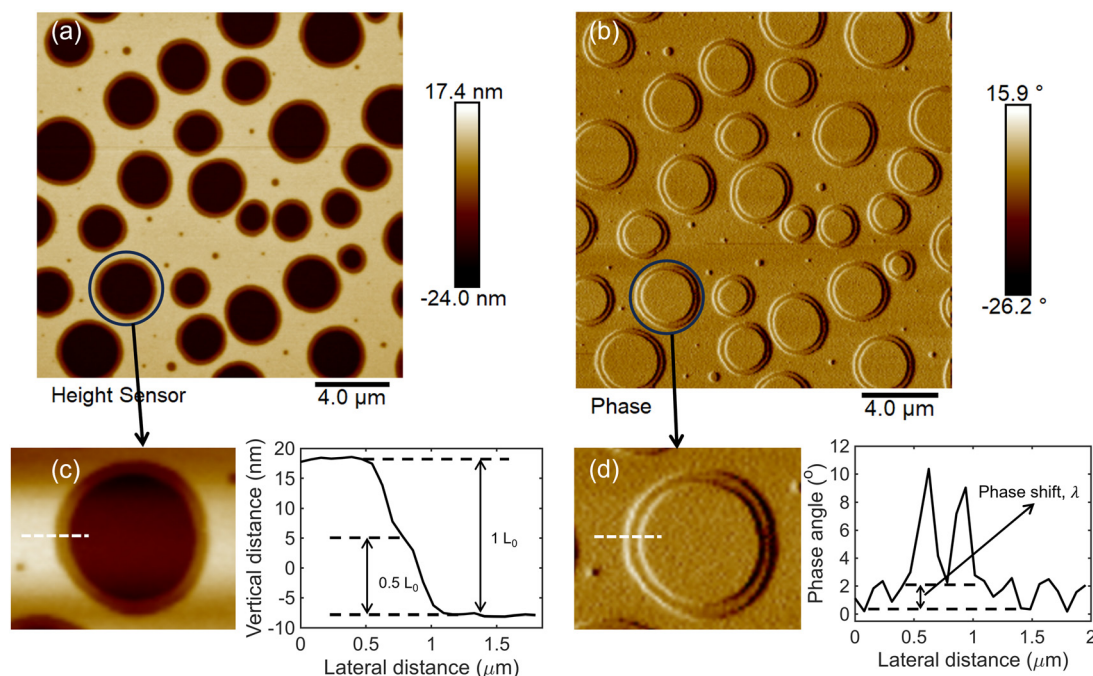


**Fig. 3** (a) The AFM colored height image of PS-*b*-PMMA showing the color of  $1L_0$  from dark brown (chocolate) at the bottom on to the surface with light brown (tan), and  $0.5L_0$ -step height with middle brown (khaki) (b) The AFM phase image of half-step lamellar domain spacing holes around one full domain spacing. (c) The hole that is magnified from the AFM height image and the line profile from the magnified AFM hole image. (d) The AFM-phase image line profile shows the phase shift at the  $0.5L_0$ -step that is different from the inside of the  $1L_0$  hole and the surface of the BCP thin film of 45 nm with microwave annealing at 10 s.

$0.5L_0$  are observed as an inflection in the height profile; however, it appears visibly small as the line profile spans  $4.5\ \mu\text{m}$ , much larger than the  $\sim 0.15\ \mu\text{m}$  rim width. Upon further microwave annealing, the surface holes become progressively larger, and inter-connected, becoming similar to the spinodal-like morphology, as shown in Fig. 4a and b at 15 s.

Two different film thicknesses are studied in the same regime of the hole-forming degree of thickness incommensuration. The thin films with 45 nm and 55 nm thicknesses show the same trend of developing increasingly larger holes with a microwave annealing time of up to 15 s. In addition to the hole-in-hole terrace formations, when the BCP film thickness  $h = 35\ \text{nm}$ , in an island formation regime, concentric island-on-island terraces are formed as shown in Fig. 5a, analogous to the concentric hole-in-hole terraces of Fig. 4.

These islands also have two layers, each with  $0.5L_0$  height, measured from the AFM height image and shown in the line height profile in Fig. 5a at 35 nm. More generally, as the thickness of the BCP thin film from this island-formation regime is increased, concentric  $0.5L_0$  hole-in-hole formations are observed at cast-film thicknesses of  $h = 45\ \text{nm}$ ,  $h = 55\ \text{nm}$ , and  $h = 120\ \text{nm}$  respectively, shown as a compilation of 10 s microwave annealing time in Fig. 5b, c, and d, respectively. The results indicate that the formation of quantized  $0.5L_0$  height concentric terraces is not an isolated phenomenon, but a more universal feature of this BCP film system. The total step heights matched the long-time oven annealed  $L_0$ , provided the microwave annealing time is 8 s.

### Anomalous PS-*b*-PMMA BCP domain stretching

Longer microwave annealing times, and with its concurrent increase of temperature, not only produce a larger hole size as shown in Fig. 6a and b but also significantly increase overall domain spacing,  $L_0(t)$ . Fig. 6a shows the change in the lamellar domain spacing of BCP thin films for the as-cast film thicknesses of  $h = 45\ \text{nm}$  and  $h = 55\ \text{nm}$ , after microwave annealing, as inferred from the AFM surface feature height, post-quenching (vitrification) to room temperature. The domain spacing  $L_0(t)$ , as measured by the surface feature height in quenched samples, increases with the microwave annealing time, in contrast to the domain spacing during thermal oven annealing which is limited to its equilibrium value. The quenched-in lamellar domain spacing of the BCP thin film increases monotonically and substantially with increasing microwave annealing times: 8 s, 10 s, 12 s, and 15 s as shown in Fig. 6a, which is correlated to the substrate's (B-doped Si wafer) rapid rise in temperature shown in Fig. 2a.

This increment of the domain spacing in  $L_0$  (33 nm@15 s@ $T(t) \sim 270\ ^\circ\text{C}$ ) from  $L_0$  (26 nm@8 s@ $181\ ^\circ\text{C}$ ) in the  $h = 45\ \text{nm}$  film is about 25%, which is well beyond the SSL theory prediction of  $\sim 10\%$  domain swelling based on  $\chi_{\text{ps-pmma}}(T)$  change (see below). Notably, Baldrian *et al.*<sup>61</sup> obtained 100% domain spacing increment in the 150–200  $^\circ\text{C}$  temperature window for 40k–40k PS-*b*-PMMA, and suggested their system was in the WSL regime. Yet, it is wellknown that the interfacial width of PS-*b*-PMMA is approximately  $\sim 5\ \text{nm}$  in this tempera-





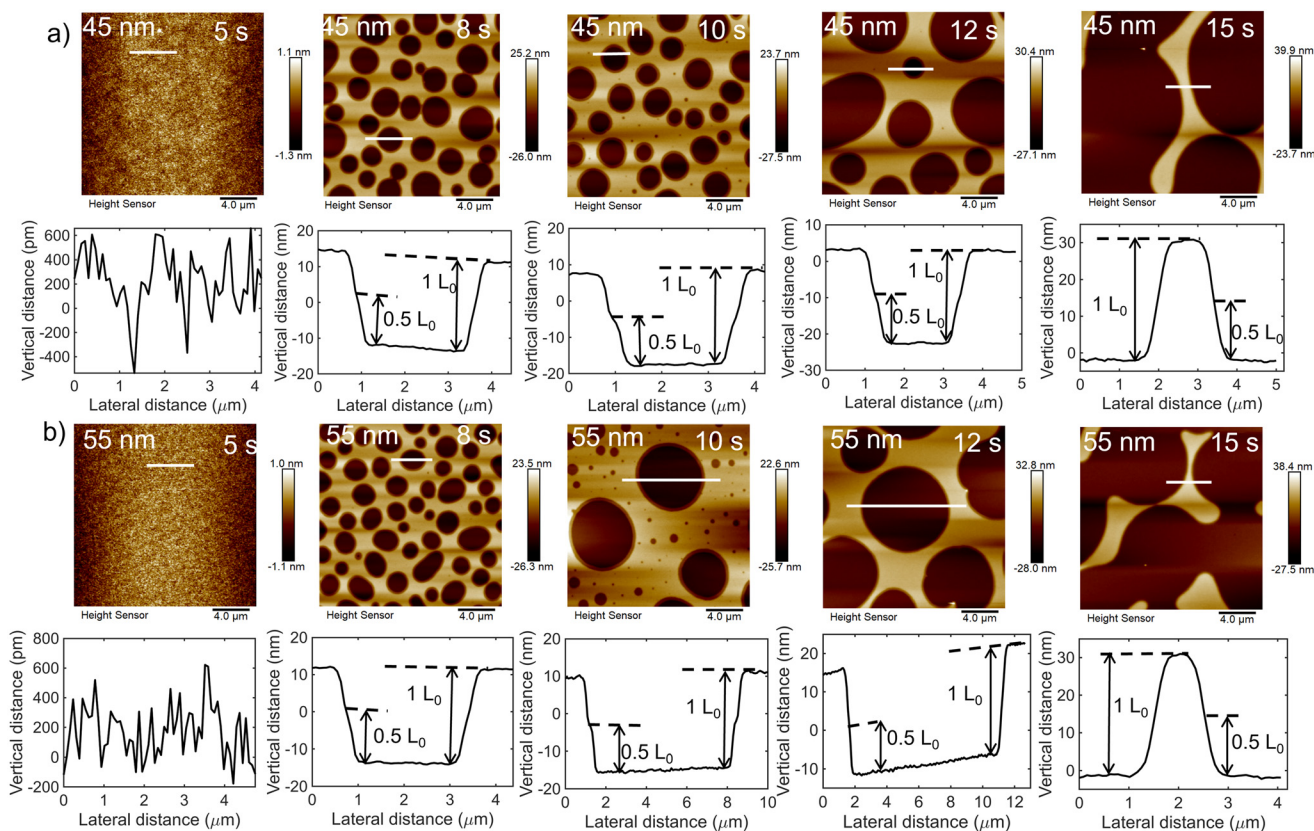


**Fig. 4** (a and b) The microwave annealing of BCP 45 nm and 55 nm thin films recorded at 5 s, 8 s, 10 s, 12 s, and 15 s: no surface holes present at 5 s, hole-in-hole terraces are created at 8 s, the average hole-in-hole diameters grow and continue at 10 s and 12 s, and holes interconnect and thus no longer exist at 15 s. The concentric terraces are more clearly observed at higher magnifications as was previously shown in Fig. 3, but can still be seen as inflection points in these line profiles.

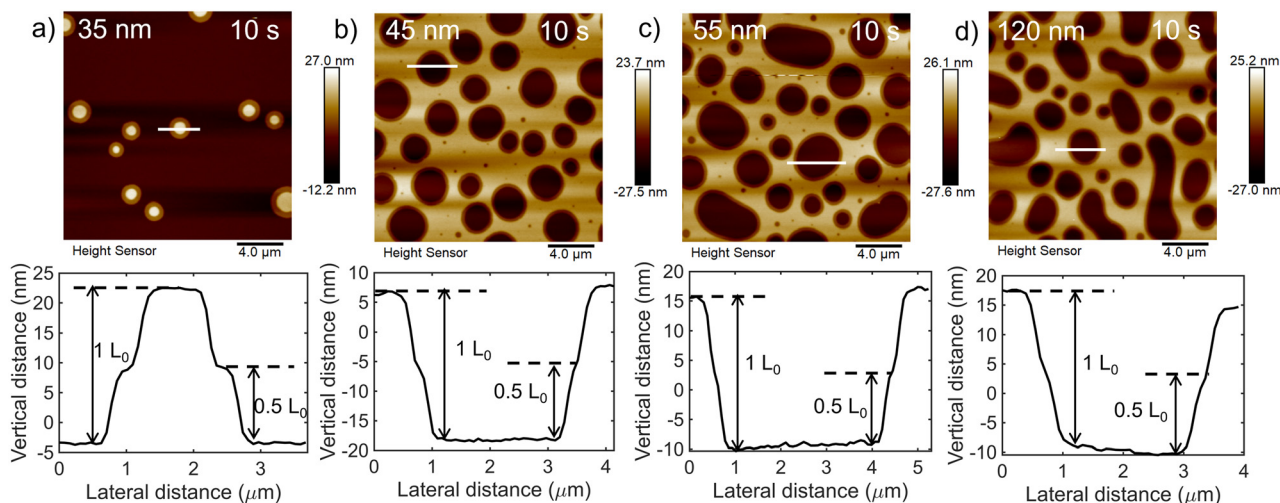


**Fig. 5** BCP thin films with thicknesses of 10 s microwave annealed of (a) 35 nm, (b) 45 nm, (c) 55 nm, and (d) 120 nm; island-on-island terrace formation of concentric  $0.5L_0$  islands at 35 nm versus concentric  $0.5L_0$  holes: 45 nm, 55 nm, and 120 nm, respectively.

ture window of 150–200 °C by neutron reflection and SANS, which matches well with the SSL assumption of a narrow interface assumption (NIA) width.

Using the phenomenological temperature dependence of  $\chi_{ps-pmma}(T) = 0.028 + 3.9/T$  (K),<sup>64</sup> we obtain an estimate of  $\chi_{ps-pmma}(@275\text{ °C}) = 0.035$ , and  $\chi N \approx 17$  for our longest micro-





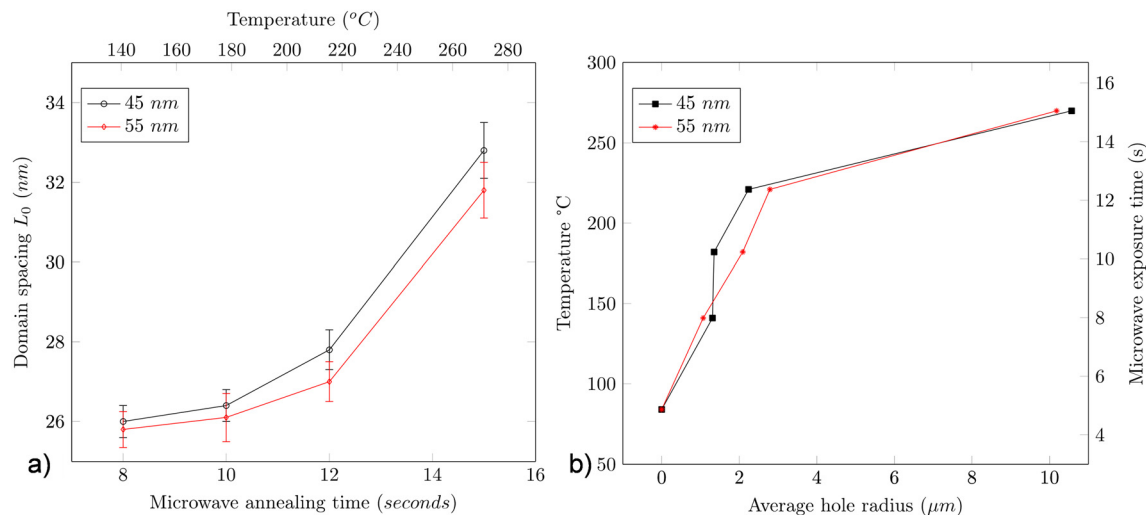


**Fig. 6** (a) TA  $L_0$  that is 26 nm increases substantially for both  $h = 45$  nm and  $h = 55$  nm PS-*b*-PMMA films by increasing the microwave annealing time from 8 s to 15 s. See the text for discussion. The corresponding temperatures of the microwave annealing time for 8 s, 10 s, 12 s, and 15 s are respectively 141 °C, 182 °C, 221 °C, and 270 °C. (b) The average hole radius at 8 s of microwave annealing continuously increases with the increment of the microwave annealing time up to 15 s.

wave annealed film of 15 s. (Other forms of the temperature-dependent equation for  $\chi_{\text{ps-pmma}}(T)$  reported in the literature do not give a significantly different value of this product, so we do not elaborate on them.) Assuming the conventional notion that  $\chi N > 50$  defines SSL, and WSL by  $10.495 < \chi N < 12.5$ , we can conclude that our PS-*b*-PMMA system at the elevated temperature is in an “intermediate” segregation regime  $12.5 \leq \chi N \leq 50$  rather than WSL, defined by a domain scaling that is larger than SSL (at least as per our results, and possibly Baldrian *et al.*<sup>61</sup>), but wherein interfacial widths match SSL predictions. This “intermediate segregation” and cross-over from the WSL to SSL regime has been previously discussed and explored by Matsen and Bates.<sup>65,66</sup> Mechanistically, this is based on the temperature dependence of  $\chi$  variation, possibly due to a synergistic combination of reduced enthalpic barrier from the enthalpic contribution of  $\chi$  scaling as  $\chi \sim 1/T$ , and high mobility arising from the diffusive motion of the chains at elevated temperatures, to cross between domain layers leading to an increased the interfacial chain-junction density. At these elevated temperatures,  $\chi$  is reduced along with the interfacial tension, allowing the chains to be more mobile, thereby allowing them to pack closer to each other near the junctions at the interface, increasing the degree of chain stretching and in turn the domain size. Such close packing would normally increase enthalpic energy per domain, but under the present conditions, it is balanced due to the reduced  $\chi$ . Such a state of ordering may be driven by a highly non-equilibrium effect associated with an anticipated rapidly evolving spatio-temporal  $z$ -temperature gradient evolution within the confined BCP film thickness.

Notably, the percentage increase in the domain size at any given microwave annealing time relative to the lowest annealing time of 8 s, e.g., domain size at 15 s annealing relative to 8 s is approximately the same in both films, with domain swell-

ing ~25% for both the  $h = 45$  nm (32.6 nm@15 s vs. 26 nm@8 s) and the  $h = 55$  nm (31.8@15 s vs. 25.7@8 s) films. However absolute domain spacings appear higher in the more confined 45 nm film compared to the 55 nm film. This suggests that the relative thermal expansion as a function of temperature can be normalized by its film thickness for a more universal-like behavior, and thereby reflective of a common chain-stretching molecular mechanism. The average hole diameters of  $L_{\text{ml}51}$  at 45 nm and 55 nm are also studied with annealing time and are shown in Fig. 6b. The average hole radius grows steadily as the temperature increases for both thicknesses, due to the dynamic (constantly increasing) temperature increment. Notably, the kinetics of hole size increment in films of 45 nm versus 55 nm are roughly the same, so that the “feature-size” in both the out-of-plane direction (domain swelling *via* hole depth kinetics data) and in-plane dimension (hole diameter expansion kinetics) has similar behavior for the two different film thicknesses.

#### Comparative varied substrate heating rate on BCP ordering

Fig. 7a demonstrates how the temperature of the high-resistivity B-doped Si substrate, *P-type2*, changes with microwave annealing time, using two different sized substrates heated by mainly microwave energy absorption, which is proportional to the substrate size, and dissipated rapidly internally by phonons (thermal conduction), which is useful to control the temperature gradient affecting the final film morphology evolution. The temperature gradient for the smaller wafer size of 150 cm<sup>2</sup> substrate, named *Substrate1*, is 18 °C s<sup>-1</sup> while that for the larger wafer size of 314 cm<sup>2</sup>, substrate, named *Substrate2*, is 13.5 °C s<sup>-1</sup> as shown in Fig. 7b.

Microwave annealing of PS-*b*-PMMA (25 K–26 K) BCP thin films on *Substrate2*, which has a smaller temperature increase gradient of 13.5 °C s<sup>-1</sup>, was also studied. Notably, the surface



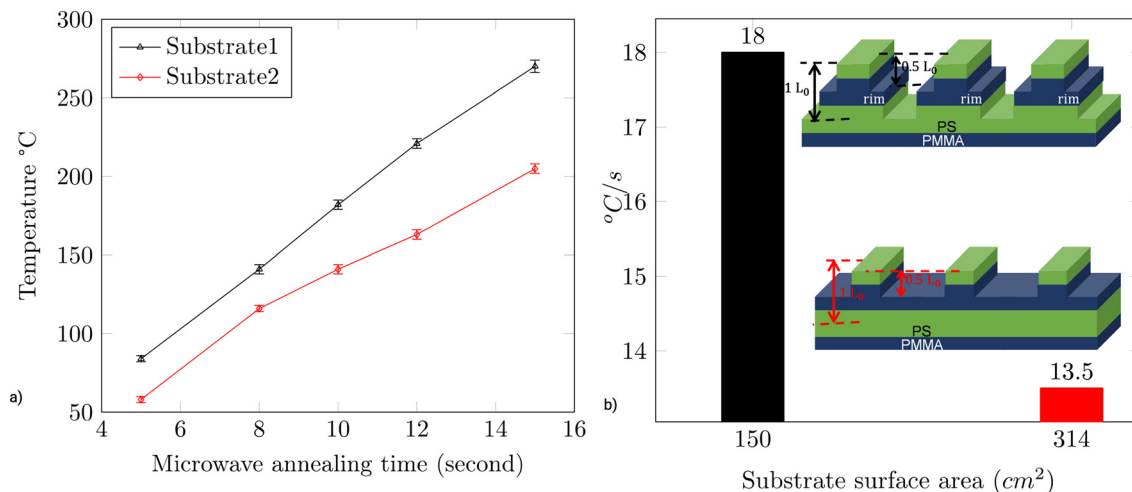


**Fig. 7** (a) Temperature of the BCP thin film's substrate, high-resistivity B-doped silicon wafer, *P-type2*, named *Substrate1* and *Substrate2* is recorded starting from 5 s until 15 s. (b) *Substrate1*, which has an area of 150 cm² and *Substrate2* having 314 cm² showed average temperature gradients of 18 °C s<sup>-1</sup> and 13.5 °C s<sup>-1</sup>, respectively.

structures of PS-*b*-PMMA on *Substrate2* exhibited only half-domain ( $0.5L_0$ ) morphologies. This observation supports our hypothesis that a rapid temperature gradient sharper than 13.5 °C s<sup>-1</sup> is needed at the substrate–film interface in order to create the rim-like island-on-island or hole-in-hole structures.

Fig. 8a shows the 45 nm thin film microwave annealed films for 8 s, which showed only  $0.5L_0$  height holes, also shown in the line height profile with heights of 12.5 nm (Fig. 8a). After 15 s of microwave annealing, the BCP films still developed the  $0.5L_0$  holes with an increased height of 15 nm due to the

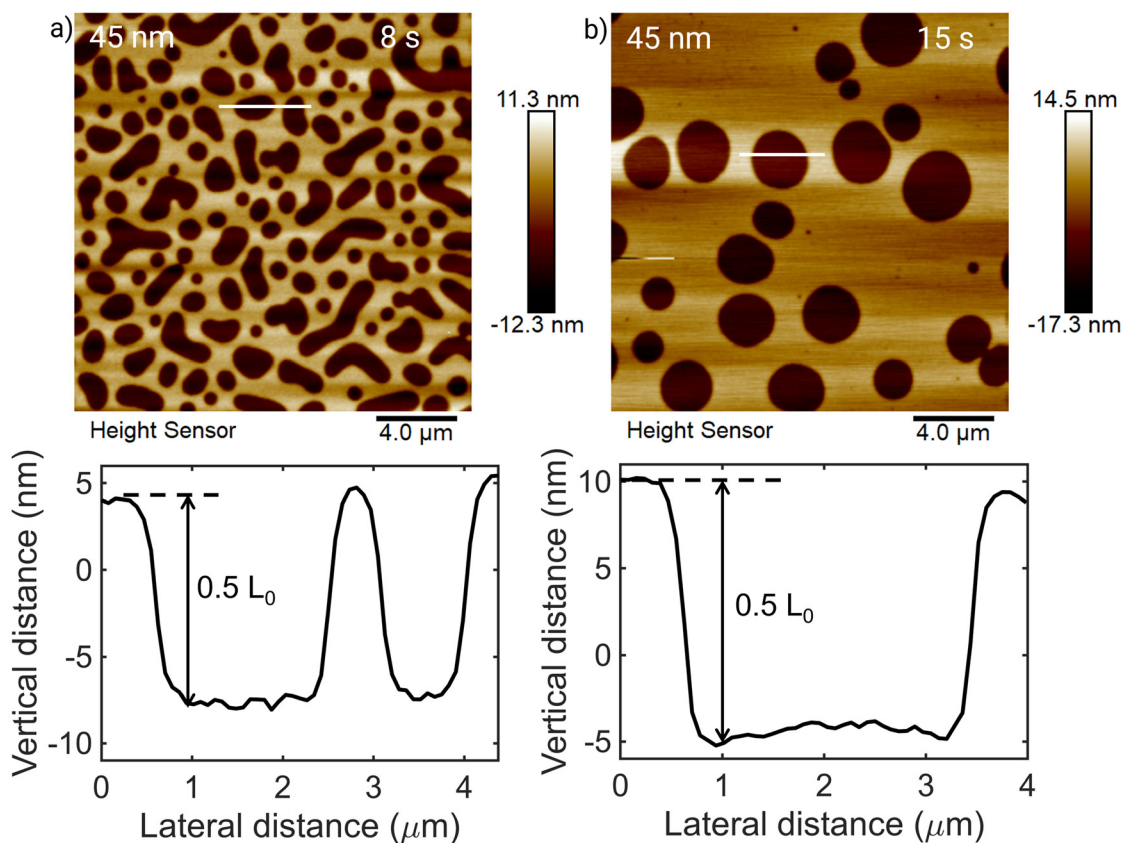


**Fig. 8** Surface morphology on *Substrate2*, with a heating rate of 13.5 °C s<sup>-1</sup>, which created only  $0.5L_0$  without rims for 45 nm in (a) 8 s and (b) 15 s.



attainment of a higher temperature (as demonstrated in Fig. 8b). The increase in the hole heights ( $0.5L_0$ ) is consistent with that observed during annealing on substrate1 ( $1L_0$ ), *i.e.*, the heating profile for our substrates shows the temporal rise of temperature for both substrates. These rates are discernibly higher than the annealing rates of BCP films in traditional thermal vacuum annealing ovens.

Temperature gradients with rates between  $18\text{ }^{\circ}\text{C s}^{-1}$  and  $13.5\text{ }^{\circ}\text{C s}^{-1}$  create mixed morphologies with only  $0.5L_0$  islands or holes and rim-like island-on-island and hole-in-hole morphologies, as shown in the ESI.† The intermediate heating rate of the substrate allowed the BCP films to create half-domain spacing features, islands, or holes along with island-on-island and hole-in-hole morphologies, as shown in Fig. S6 and S7,† which can be attributed to the slower temperature increment. (While outside the scope of our study, this has to do with not only the substrate type, but also where microwave antinodes have the highest amplitudes, schematically shown in Fig. 2c, which depends on substrate dimensions.) These island-on-island and hole-in-hole morphologies are also formed in  $Lml_{36.5}$  thin films, which makes these novel features common to other molecular masses of PS-*b*-PMMA BCP thin films and are demonstrated in Fig. S4 and S5.†

For comparison, we also studied BCP PS-*b*-P2VP,  $Lml_{50}^*$  thin films with a much higher interaction parameter  $\chi_{\text{ps-p2vp}} \cong 0.11@150\text{ }^{\circ}\text{C}$ , annealed using microwaves for 10 s on the  $18\text{ }^{\circ}\text{C s}^{-1}$  rise substrate; however, no hole-in-hole or island-on-island features were produced due to the fact that PS and P2VP (substrate wetting) have significantly larger interfacial surface energy difference,<sup>67,68</sup> which does not become equal (neutrality at the air boundary is needed for  $0.5L_0$ ) at high temperatures like PS-*b*-PMMA BCP films, resulting in only  $1L_0$  islands and holes, as shown in Fig. S3.† Nevertheless, the kinetics of ordering in even PS-*b*-P2VP BCP films on microwave-absorbing substrates is much faster than oven annealing in all cases. This suggests that concentric rim-like morphologies are prone to be observed in block copolymers having similar air interface surface energies with one block preferred at the substrate interface, under high temperature-gradient heating. Microwave processing thus provides a fast, clean, and economical method to create ordered parallel lamellar BCP thin films within seconds and with unique surface morphologies, which may be relevant to industrial processing requiring such surface morphologies such as for next-generation laser light scattering standards.

## 4. Discussions

BCP thin films can form a variety of thermodynamic equilibrium morphologies, such as spherical, cylindrical, lamellar, and gyroid structures. These morphologies depend on the volume fractions of the constituent blocks (block A and block B, ( $f_{A/B}$ )), the segregation strength,  $\chi N_T$ ,<sup>69</sup> the degree of overall polymerization,  $N_T$ , and the Flory-Huggins interaction parameter,  $\chi_{AB}$ . Microwave annealing can sharply and rapidly

increase the temperature of the underlying substrate, resulting in high-temperature gradients in the *z*-direction, *i.e.*, film thickness direction. The surface structures of BCP thin films are formed due to the interactions at the free surface (top) and substrate (bottom) interfaces with the BCP thin film. Poly(styrene) (PS) and poly(methyl methacrylate) (PMMA) have similar surface energies, differing by only  $0.1\text{ dyn cm}^{-1}$  at room temperature, with PS having the lower surface energy.<sup>70</sup> This difference in interfacial energies nearly vanishes at  $225\text{ }^{\circ}\text{C}$ , creating a neutral-free surface.<sup>71</sup> We hypothesize that the similar surface energies of PS and PMMA at a high *z*-temperature gradient are the main reason for the creation of  $0.5L_0$  step concentric morphologies, which are not observed for PS-*b*-P2VP (25 K–25 K). In  $Lml_{36.5}$  BCP films, the same morphologies as in  $Lml_{51}$  are observed. We further determined that the hole-in-hole and island-on-island morphologies have the same incommensurability conditions as those of single-layered islands or hole morphologies in thermally annealed films. The total amount of polymer (block copolymer) remains constant during the formation of the multi-tiered holes. Even in the formation of traditional “uni-depth” holes in ordered block copolymer thin films, the total mass of the BCP is conserved, regardless of whether they are in the SSL or WSL limit. Essentially, the cumulative hole depth volumes are compensated by an elevation of the surrounding contiguous phase by an equivalent volume amount through melt diffusion-driven ordering.

We now ask the question why BCP thin films at equilibrium with non-integral thickness with  $L_0$  produce surface topographies such as island-on-island or hole-in-hole structures by microwave annealing. We hypothesize this unique rim-on-rim morphology is created in response to the steep dynamic temperature gradient in the film induced by the microwave absorbing substrate that heats the film rapidly from the bottom (for the B-doped Si substrate, only the temperature rise was found to be  $18\text{ }^{\circ}\text{C s}^{-1}$ ). Thus, the temperature of the BCP film at the outermost air interface is lower than in the BCP layer inner to it (that is closer to the heating substrate). This differential temperature produces a differential surface tension, which is higher at the air interface than in the layer inner to it. A higher surface tension at the air interface in turn increases the flexural bending modulus ( $E$ ) associated with the rim formation curvature at the air interface compared to the inner layer, *i.e.*,  $E_{\text{surface}} > E_{\text{inner layer}}$ . Since flexural modulus energy varies inversely with the rim radius,  $E \sim 1/r$ , a larger rim radius at the air interface helps lower the flexural bending energy of the rim.<sup>72–74</sup> Regarding rim evolution kinetics, the average width of  $0.5L_0$  step rims for  $L_0$  of both 45 nm and 55 nm thicknesses decreased by 50% with roughly doubling of the microwave annealing time (from about  $0.62\text{ }\mu\text{m}$  at 8 s to  $0.31\text{ }\mu\text{m}$  and  $0.33\text{ }\mu\text{m}$  at 15 s). Although the rims become almost indistinguishable after 15 s in the AFM height image, they are still visible in the AFM phase image (Fig. S1†), indicating their presence. The rim-like  $0.5L_0$  structure does not disappear even at 15 seconds due to the high-temperature gradient of  $18\text{ }^{\circ}\text{C s}^{-1}$ . However, the width of the  $0.5L_0$  step decreases with longer





annealing times (8 s, 10 s, 12 s, and 15 s), likely due to reducing the energetically unfavorable rim surface area created, in conjunction with z-temperature gradient homogenization with time. As the surface tension depends on the temperature, high-temperature gradients can, in principle, drive Marangoni patterns involving fluid flow from higher surface tension areas (top of the film) to lower surface tension areas (bottom of the film). The Marangoni effect on simple Newtonian fluids is well studied; however, Marangoni effects are generally suppressed in high-molecular-weight polymers due to their high viscosity.<sup>75,76</sup> The highly stratified ordered BCP films would suppress such Marangoni flow even more. Importantly, if macroscale z-directed Marangoni fluid flow occurred in these lamellar structured block copolymer films, all the individual phase-separated BCP layers would be quite mixed up from churning effects! However, we cannot rule out local molecular scale forces originating from “suppressed macroscale Marangoni effects” as causing the multi-tier surface holes.<sup>75,76</sup>

Notably, when we use a B-doped silicon substrate that produces a lower temperature increase of  $13.5\text{ }^{\circ}\text{C s}^{-1}$ , the rim-in-rim structure disappears in favor of only a  $0.5L_0$  hole morphology, consistent with Wilson's results of surface morphology evolution in incommensurate films with a neutral air interface and preferential (PMMA) substrate interface in ultrathin films. However, we did not test if our  $0.5L_0$  hole morphology PS-*b*-PMMA films would evolve into  $1L_0$  holes with extended microwave annealing time due to concerns of sample degradation beyond 15 s in air. In our case, far from equilibrium, rapid microwave annealing created highly stretched BCP domains in the z-direction due to the thin film confinement effects. However, we have no reason or evidence to believe that the film density below the hole layer is not the same as the bulk BCP density in this case either.

Block copolymers intrigued salient interest as materials for photonic crystals due to their ability to self-assemble, especially lamellar domains forming from block copolymer films, shown to tune optical properties. As optical implications need high-end next-generation materials, this  $0.5L_0$  rim morphology can lead to the construction of optical transmission filters or waveguides.<sup>77–79</sup> These novel BCP morphologies with the ultra-fast annealing process also show potential implications in the Internet of Things (IoT), gene delivery, and trapped drugs, in the hierarchical surface topographies with multi-purpose applications.<sup>74,80–82</sup>

## 5. Conclusions

Microwave annealing is used to rapidly create ordered periodic parallel rim-like hole-in-hole and island-on-island lamellar nanostructures. This study thoroughly examines how temperature gradients and film thickness affect domain spacing and produce surface terraces at the interfaces of BCP thin films. By microwave absorbing high-resistivity B-doped Si substrates @ $18\text{ }^{\circ}\text{C s}^{-1}$ , the BCP thin films reached an equilibrium structure in as little as 8 s, forming well-developed holes on the

interface, and we hypothesize a high z-temperature gradient is responsible for this first evidence of subsequent transient multilayered and concentric  $0.5L_0$  surface island and hole structures that split  $1L_0$  surface structure formation at higher temperature evolution until  $270\text{ }^{\circ}\text{C}$  at 15 s. Surface energetics to reduce the surface, temperature gradient homogenization and increased mobility at high temperature drive the rim widths to progressively decrease with increasing microwave annealing time. In comparison, we can achieve only  $0.5L_0$  surface structures when the substrate heating rate is  $13.5\text{ }^{\circ}\text{C s}^{-1}$ , by the mechanism of neutral air and preferential substrate interactions of BCP films. Intermediate heating rates between  $13.5\text{ }^{\circ}\text{C s}^{-1}$  and  $18\text{ }^{\circ}\text{C s}^{-1}$  create mixed morphologies, so these results are highly correlated to heating rates of the substrate and the transient nature of the temperature gradient in the film through-thickness direction. Future modeling studies can potentially lay the basis for these experimental observations, but they are out of the scope of the present study.

Another unique observation is that the 15 s microwave annealing increased the domain spacing by nearly 25% compared to the 8 s annealing, due to the concurrent lowering of the interaction parameter (enthalpic effect), enhanced chain mobility and reduced penalty for stretching of polymer chains at elevated temperatures (entropic effect). We have suggested that the system lies in an “intermediate segregation” state wherein domain stretching well exceeds the SSL theory, but the interfacial width (as confirmed from the literature) conforms to the SSL theory.

Overall, this work successfully applies microwave annealing to create hierarchical parallel lamellar morphology with interesting  $0.5L_0$  rim features in vertically split  $1L_0$  structures, with significantly enhanced domain spacing, by irradiating a microwave-absorbing high-resistivity B-doped sSi wafer at a high heating rate ( $18\text{ }^{\circ}\text{C s}^{-1}$ ). Lower heating rate conditions ( $13.5\text{ }^{\circ}\text{C s}^{-1}$ ) produce an equally interesting  $0.5L_0$  surface topography, as a simple route for attaining the uncommon  $0.5L_0$  islands and holes in PS-*b*-PMMA BCPs. With further research aimed at scaling up the method, we suggest that microwave substrate-directed self-assembly (MS-DSA) is valuable for industrial processing of BCP films for the development of unique surface topography and expanded domains in the film thickness or z-dimension.

## Disclaimer

Certain commercial equipment, instruments, or materials are identified in this paper to foster understanding. Such identification does not imply recommendation or endorsement by the National Institute of Standards and Technology, nor does it imply that the materials or equipment identified are necessarily the best available for the purpose.

## Conflicts of interest

There are no conflicts to declare.



## Data availability

The data supporting this article have been included as part of the SI.

## Acknowledgements

The authors acknowledge funding from NSF (DMR) # 1900692, Welch E-2105-20220331 and Welch V-E-0003-20230731 for all aspects of this research work.

## References

- 1 T. Thurn-Albrecht, J. Schotter, G. A. Kastle, N. Emley, T. Shibauchi, L. Krusin-Elbaum, K. Guarini, C. T. Black, M. T. Tuominen and T. P. Russell, Ultrahigh-density nanowire arrays grown in self-assembled diblock copolymer templates, *Science*, 2000, **290**(5499), 2126–2129.
- 2 P. F. Green, T. M. Christensen and T. P. Russell, Ordering at diblock copolymer surfaces, *Macromolecules*, 1991, **24**(1), 252–255.
- 3 C. J. Hawker and T. P. Russell, Block copolymer lithography: Merging “bottom-up” with “top-down” processes, *MRS Bull.*, 2005, **30**(12), 952–966.
- 4 X. Gu, I. Gunkel, A. Hexemer and T. P. Russell, Controlling domain spacing and grain size in cylindrical block copolymer thin films by means of thermal and solvent vapor annealing, *Macromolecules*, 2016, **49**(9), 3373–3381.
- 5 T. P. Russell, X-ray and neutron reflectivity for the investigation of polymers, *Mater. Sci. Rep.*, 1990, **5**(4), 171–271.
- 6 S. Ouk Kim, H. H. Solak, M. P. Stoykovich, N. J. Ferrier, J. J. De Pablo and P. F. Nealey, Epitaxial self-assembly of block copolymers on lithographically defined nanopatterned substrates, *Nature*, 2003, **424**(6947), 411–414.
- 7 P. Mansky, Y. Liu, E. Huang, T. P. Russell and C. Hawker, Controlling polymer-surface interactions with random copolymer brushes, *Science*, 1997, **275**(5305), 1458–1460.
- 8 K. Sharma, A. Agrawal, A. Masud, S. K. Satija, J. F. Ankner, J. F. Douglas and A. Karim, Hiking down the Free Energy Landscape Using Sequential Solvent and Thermal Processing for Versatile Ordering of Block Copolymer Films, *ACS Appl. Mater. Interfaces*, 2023, **15**(17), 21562–21574.
- 9 S. H. Anastasiadis, T. P. Russell, S. K. Satija and C. F. Majkrzak, Neutron reflectivity studies of the surface-induced ordering of diblock copolymer films, *Phys. Rev. Lett.*, 1989, **62**(16), 1852.
- 10 S. R. Nowak and K. G. Yager, Photothermally directed assembly of block copolymers, *Adv. Mater. Interfaces*, 2020, **7**(5), 1901679.
- 11 S. H. Kim, M. J. Misner, T. Xu, M. Kimura and T. P. Russell, Highly oriented and ordered arrays from block copolymers via solvent evaporation, *Adv. Mater.*, 2004, **16**(3), 226–231.
- 12 K. Fukunaga, H. Elbs, R. Magerle and G. Krausch, Large-scale alignment of ABC block copolymer microdomains via solvent vapor treatment, *Macromolecules*, 2000, **33**(3), 947–953.
- 13 T. L. Morkved, M. Lu, A. M. Urbas, E. E. Ehrichs, H. M. Jaeger, P. Mansky and T. P. Russell, Local control of microdomain orientation in diblock copolymer thin films with electric fields, *Science*, 1996, **273**(5277), 931–933.
- 14 Z. Qiang, Y. Zhang, J. A. Groff, K. A. Cavicchi and B. D. Vogt, A generalized method for alignment of block copolymer films: solvent vapor annealing with soft shear, *Soft Matter*, 2014, **10**(32), 6068–6076.
- 15 G. Singh, K. G. Yager, B. Berry, H. C. Kim and A. Karim, Dynamic thermal field-induced gradient soft-shear for highly oriented block copolymer thin films, *ACS Nano*, 2012, **6**(11), 10335–10342.
- 16 M. Singh, W. Wu, M. N. Basutkar, J. Strzalka, A. M. Al-Enizi, J. F. Douglas and A. Karim, Ultra-fast vertical ordering of lamellar block copolymer films on unmodified substrates, *Macromolecules*, 2021, **54**(3), 1564–1573.
- 17 P. W. Majewski and K. G. Yager, Millisecond ordering of block copolymer films via photothermal gradients, *ACS Nano*, 2015, **9**(4), 3896–3906.
- 18 C. Sinturel, M. Vayer, M. Morris and M. A. Hillmyer, Solvent vapor annealing of block polymer thin films, *Macromolecules*, 2013, **46**(14), 5399–5415.
- 19 K. W. Gotrik and C. A. Ross, Solvothermal annealing of block copolymer thin films, *Nano Lett.*, 2013, **13**(11), 5117–5122.
- 20 K. Sharma, M. Singh, S. K. Satija, J. F. Ankner, J. F. Douglas and A. Karim, Transient Interfacial Pattern Formation in Block Copolymer Thin Films via Sequential Thermal and Solvent Immersion Annealing, *ACS Appl. Mater. Interfaces*, 2024, **16**(12), 15569–15585.
- 21 X. Zhang, K. D. Harris, N. L. Y. Wu, J. N. Murphy and J. M. Buriak, Fast assembly of ordered block copolymer nanostructures through microwave annealing, *ACS Nano*, 2010, **4**(11), 7021–7029.
- 22 C. Jin, J. N. Murphy, K. D. Harris and J. M. Buriak, Deconvoluting the mechanism of microwave annealing of block copolymer thin films, *ACS Nano*, 2014, **8**(4), 3979–3991.
- 23 C. M. Bates, M. J. Maher, D. W. Janes, C. J. Ellison and C. G. Willson, Block copolymer lithography, *Macromolecules*, 2014, **47**(1), 2–12.
- 24 Y. A. Elabd and M. A. Hickner, Block copolymers for fuel cells, *Macromolecules*, 2011, **44**(1), 1–11.
- 25 U. Aslan and T. Çağın, Influence of H-Content on Thermo-Mechanical Properties of NiAl Alloys, in *Materials Science Forum*, Trans Tech Publ, 2018, pp. 224–228.
- 26 S. P. Nunes, Block copolymer membranes for aqueous solution applications, *Macromolecules*, 2016, **49**(8), 2905–2916.
- 27 M. Singh, A. Agrawal, W. Wu, A. Masud, E. Armijo, D. Gonzalez, S. Zhou, T. Terlier, C. Zhu and J. Strzalka, Soft-Shear-Aligned Vertically Oriented Lamellar Block Copolymers for Template-Free Sub-10 nm Patterning and



- Hybrid Nanostructures, *ACS Appl. Mater. Interfaces*, 2022, **14**(10), 12824–12835.
- 28 J. Lee, C. Y. Koh, J. P. Singer, S. Jeon, M. Maldovan, O. Stein and E. L. Thomas, 25th anniversary article: ordered polymer structures for the engineering of photons and phonons, *Adv. Mater.*, 2014, **26**(4), 532–569.
  - 29 S. P. Samant, C. A. Grabowski, K. Kisslinger, K. G. Yager, G. Yuan, S. K. Satija, M. F. Durstock, D. Raghavan and A. Karim, Directed self-assembly of block copolymers for high breakdown strength polymer film capacitors, *ACS Appl. Mater. Interfaces*, 2016, **8**(12), 7966–7976.
  - 30 A. P. Smith, J. F. Douglas, J. C. Meredith, E. J. Amis and A. Karim, High-throughput characterization of pattern formation in symmetric diblock copolymer films, *J. Polym. Sci., Part B: Polym. Phys.*, 2001, **39**(18), 2141–2158.
  - 31 A. P. Smith, A. Sehgal, J. F. Douglas, A. Karim and E. J. Amis, Combinatorial mapping of surface energy effects on diblock copolymer thin film ordering, *Macromol. Rapid Commun.*, 2003, **24**(1), 131–135.
  - 32 M. J. Maher, J. L. Self, P. Stasiak, G. Blachut, C. J. Ellison and M. W. Matsen, Structure, Stability, and Reorganization of 0.5 L 0 Topography in Block Copolymer Thin Films, *ACS Nano*, 2016, **10**(11), 10152–10160.
  - 33 M. J. Maher, C. M. Bates, G. Blachut, S. Sirard, J. L. Self, M. C. Carlson, L. M. Dean, J. D. Cushen, W. J. Durand and C. O. Hayes, Interfacial design for block copolymer thin films, *Chem. Mater.*, 2014, **26**(3), 1471–1479.
  - 34 S. Kim, C. M. Bates, A. Thio, J. D. Cushen, C. J. Ellison, C. G. Willson and F. S. Bates, Consequences of surface neutralization in diblock copolymer thin films, *ACS Nano*, 2013, **7**(11), 9905–9919.
  - 35 G. Coulon, B. Collin, D. Ausserre, D. Chatenay and T. P. Russell, Islands and holes on the free surface of thin diblock copolymer films. I. Characteristics of formation and growth, *J. Phys.*, 1990, **51**(24), 2801–2811.
  - 36 A. P. Smith, J. F. Douglas, E. J. Amis and A. Karim, Effect of temperature on the morphology and kinetics of surface pattern formation in thin block copolymer films, *Langmuir*, 2007, **23**(24), 12380–12387.
  - 37 W. H. Sutton, Microwave processing of materials, *MRS Bull.*, 1993, **18**(11), 22–29.
  - 38 S. Horikoshi and N. Serpone, Microwave frequency effect (s) in organic chemistry, *Mini-Rev. Org. Chem.*, 2011, **8**(3), 299–305.
  - 39 V. Palma, D. Barba, M. Cortese, M. Martino, S. Renda and E. Meloni, Microwaves and heterogeneous catalysis: A review on selected catalytic processes, *Catalysts*, 2020, **10**(2), 246.
  - 40 D. Adam, Microwave chemistry: Out of the kitchen, *Nature*, 2003, **421**(6923), 571–573.
  - 41 S. W. Liu and J. P. Wightman, Decomposition of simple alcohols, ethers and ketones in a microwave discharge, *J. Appl. Chem. Biotechnol.*, 1971, **21**(6), 168–172.
  - 42 L. A. Campanone and N. E. Zaritzky, Mathematical analysis of microwave heating process, *J. Food Eng.*, 2005, **69**(3), 359–368.
  - 43 D. T. W. Toolan, K. Adlington, A. Isakova, A. Kalamiotis, P. Mokarian-Tabari, G. Dimitrakis, C. Dodds, T. Arnold, N. J. Terrill and W. Bras, Selective molecular annealing: in situ small angle X-ray scattering study of microwave-assisted annealing of block copolymers, *Phys. Chem. Chem. Phys.*, 2017, **19**(31), 20412–20419.
  - 44 P. Mokarian-Tabari, C. Cummins, S. Rasappa, C. Simao, C. M. Sotomayor Torres, J. D. Holmes and M. A. Morris, Study of the kinetics and mechanism of rapid self-assembly in block copolymer thin films during solvo-microwave annealing, *Langmuir*, 2014, **30**(35), 10728–10739.
  - 45 T. Higuchi, M. Shimomura and H. Yabu, Reorientation of microphase-separated structures in water-suspended block copolymer nanoparticles through microwave annealing, *Macromolecules*, 2013, **46**(10), 4064–4068.
  - 46 D. Borah, M. T. Shaw, J. D. Holmes and M. A. Morris, Sub-10 nm feature size PS-*b*-PDMS block copolymer structures fabricated by a microwave-assisted solvothermal process, *ACS Appl. Mater. Interfaces*, 2013, **5**(6), 2004–2012.
  - 47 X. Shi, X. Wang, Y. Wang and Y. Wang, Producing nanoporosities in block copolymers within 30 s by microwave-booster selective swelling, *Macromolecules*, 2020, **53**(9), 3619–3626.
  - 48 D. Borah, R. Sentharamaikkannan, S. Rasappa, B. Kosmala, J. D. Holmes and M. A. Morris, Swift nanopattern formation of PS-*b*-PMMA and PS-*b*-PDMS block copolymer films using a microwave assisted technique, *ACS Nano*, 2013, **7**(8), 6583–6596.
  - 49 Z. Qiang, C. Ye, K. Lin, M. L. Becker, K. A. Cavicchi and B. D. Vogt, Evolution in surface morphology during rapid microwave annealing of PS-*b*-PMMA thin films, *J. Polym. Sci., Part B: Polym. Phys.*, 2016, **54**(15), 1499–1506.
  - 50 S. Park, M. P. Stoykovich, R. Ruiz, Y. Zhang, C. T. Black and P. F. Nealey, Directed assembly of lamellae-forming block copolymers by using chemically and topographically patterned substrates, *Adv. Mater.*, 2007, **19**(4), 607–611.
  - 51 C. C. Liu, A. Ramírez-Hernández, E. Han, G. S. W. Craig, Y. Tada, H. Yoshida, H. Kang, S. Ji, P. Gopalan and J. J. De Pablo, Chemical patterns for directed self-assembly of lamellae-forming block copolymers with density multiplication of features, *Macromolecules*, 2013, **46**(4), 1415–1424.
  - 52 S. Kim, P. F. Nealey and F. S. Bates, Directed assembly of lamellae forming block copolymer thin films near the order-disorder transition, *Nano Lett.*, 2014, **14**(1), 148–152.
  - 53 A. M. Welfander, H. Kang, K. O. Stuenkel, H. H. Solak, M. Müller, J. J. de Pablo and P. F. Nealey, Rapid directed assembly of block copolymer films at elevated temperatures, *Macromolecules*, 2008, **41**(8), 2759–2761.
  - 54 S. O. Kim, B. H. Kim, K. Kim, C. M. Koo, M. P. Stoykovich, P. F. Nealey and H. H. Solak, Defect structure in thin films of a lamellar block copolymer self-assembled on neutral homogeneous and chemically nanopatterned surfaces, *Macromolecules*, 2006, **39**(16), 5466–5470.
  - 55 J. Heier, E. J. Kramer, J. Groenewold and G. H. Fredrickson, Kinetics of individual block copolymer island formation





- and disappearance near an absorbing boundary, *Macromolecules*, 2000, **33**(16), 6060–6067.
- 56 T. Thurn-Albrecht, R. Steiner, J. DeRouchey, C. M. Stafford, E. Huang, M. Bal, M. Tuominen, C. J. Hawker and T. P. Russell, Nanoscopic templates from oriented block copolymer films, *Adv. Mater.*, 2000, **12**(11), 787–791.
  - 57 A. B. Croll, M. V. Massa, M. W. Matsen and K. Dalnoki-Veress, Droplet shape of an anisotropic liquid, *Phys. Rev. Lett.*, 2006, **97**(20), 204502.
  - 58 M. J. Maher, J. L. Self, P. Stasiak, G. Blachut, C. J. Ellison, M. W. Matsen, C. M. Bates and C. G. Willson, Structure, Stability, and Reorganization of 0.5 L0 Topography in Block Copolymer Thin Films, *ACS Nano*, 2016, **10**(11), 10152–10160, DOI: [10.1021/acsnano.6b05390](https://doi.org/10.1021/acsnano.6b05390).
  - 59 F. S. Bates and G. H. Fredrickson, Block copolymer thermodynamics: theory and experiment, *Annu. Rev. Phys. Chem.*, 1990, **41**(1), 525–557.
  - 60 D. J. Pochan, E. K. Lin, S. K. Satija and W. I. Wu, Thermal expansion of supported thin polymer films: A direct comparison of free surface vs total confinement, *Macromolecules*, 2001, **34**(9), 3041–3045.
  - 61 J. Holoubek, F. Lednický and J. Baldrian, Non-equilibrium self-assembled structures in thick PS-b-PMMA copolymer films, *Eur. Polym. J.*, 2006, **42**(10), 2236–2246.
  - 62 E. T. Thostenson and T. Chou, Microwave and conventional curing of thick-section thermoset composite laminates: experiment and simulation, *Polym. Compos.*, 2001, **22**(2), 197–212.
  - 63 A. Masud, W. Wu, M. Singh, W. Tonny, A. Ammar, K. Sharma, J. W. Strzalka, T. Terlier, J. F. Douglas and A. Karim, Solvent processing and ionic liquid-enabled long-range vertical ordering in block copolymer films with enhanced film stability, *Macromolecules*, 2021, **54**(18), 8512–8525.
  - 64 T. P. Russell, R. P. Hjelm Jr and P. A. Seeger, Temperature dependence of the interaction parameter of polystyrene and poly (methyl methacrylate), *Macromolecules*, 1990, **23**(3), 890–893.
  - 65 M. W. Matsen and F. S. Bates, Unifying weak-and strong-segregation block copolymer theories, *Macromolecules*, 1996, **29**(4), 1091–1098.
  - 66 M. W. Matsen and F. S. Bates, Block copolymer microstructures in the intermediate-segregation regime, *J. Chem. Phys.*, 1997, **106**(6), 2436–2448.
  - 67 S. Ji, C. C. Liu, J. G. Son, K. Gotrik, G. S. W. Craig, P. Gopalan, F. J. Himpsel, K. Char and P. F. Nealey, Generalization of the use of random copolymers to control the wetting behavior of block copolymer films, *Macromolecules*, 2008, **41**(23), 9098–9103.
  - 68 B. B. Sauer and G. T. Dee, Surface tension and melt cohesive energy density of polymer melts including high melting and high glass transition polymers, *Macromolecules*, 2002, **35**(18), 7024–7030.
  - 69 F. S. Bates and G. H. Fredrickson, Block copolymers—designer soft materials, *Phys. Today*, 2000, **52**, 32–38.
  - 70 T. P. Russell, G. Coulon, V. R. Deline and D. C. Miller, Characteristics of the surface-induced orientation for symmetric diblock PS/PMMA copolymers, *Macromolecules*, 1989, **22**(12), 4600–4606.
  - 71 P. Mansky, T. P. Russell, C. J. Hawker, J. Mays, D. C. Cook and S. K. Satija, Interfacial segregation in disordered block copolymers: effect of tunable surface potentials, *Phys. Rev. Lett.*, 1997, **79**(2), 237.
  - 72 V. Bergeron, A. I. Jimenez-Laguna and C. J. Radke, Hole formation and sheeting in the drainage of thin liquid films, *Langmuir*, 1992, **8**(12), 3027–3032.
  - 73 J. S. Sharp, K. R. Thomas and M. P. Weir, Mechanically driven wrinkling instability in thin film polymer bilayers, *Phys. Rev. E: Stat., Nonlinear, Soft Matter Phys.*, 2007, **75**(1), 011601.
  - 74 D. P. Holmes, Elasticity and stability of shape-shifting structures, *Curr. Opin. Colloid Interface Sci.*, 2019, **40**, 118–137.
  - 75 C. V. Sternling and L. E. Scriven, Interfacial turbulence: hydrodynamic instability and the Marangoni effect, *AIChE J.*, 1959, **5**(4), 514–523.
  - 76 L. E. Scriven and C. V. Sternling, The marangoni effects, *Nature*, 1960, **187**(4733), 186–188.
  - 77 Y. Fan, J. J. Walish, S. Tang, B. D. Olsen and E. L. Thomas, Defects, solvent quality, and photonic response in lamellar block copolymer gels, *Macromolecules*, 2014, **47**(3), 1130–1136.
  - 78 T. Deng, C. Chen, C. Honeker and E. L. Thomas, Two-dimensional block copolymer photonic crystals, *Polymer*, 2003, **44**(21), 6549–6553.
  - 79 J. Yoon, W. Lee and E. L. Thomas, Self-assembly of block copolymers for photonic-bandgap materials, *MRS Bull.*, 2005, **30**(10), 721–726.
  - 80 K. Park, H. M. Jin, K. Kwon, J. H. Kim, H. Yun, K. H. Han, T. Yun, S. O. Kim and H. Jung, Large-Area Alignment of Supramolecular Columns by Photothermal Laser Writing, *Adv. Mater.*, 2020, **32**(36), 2002620.
  - 81 J. H. Kim, S. Jeon, J. H. In, S. Nam, H. M. Jin, K. H. Han, G. G. Yang, H. J. Choi, K. M. Kim and J. Shin, Nanoscale physical unclonable function labels based on block copolymer self-assembly, *Nat. Electron.*, 2022, **5**(7), 433–442.
  - 82 G. G. Yang, H. J. Choi, S. Li, J. H. Kim, K. Kwon, H. M. Jin, B. H. Kim and S. O. Kim, Intelligent block copolymer self-assembly towards IoT hardware components, *Nat. Rev. Electr. Eng.*, 2024, **1**(2), 124–138.
  - 83 A. Ammar, J. D. Smith, U. Aslan, V. Balan, M. L. Robertson and A. Karim, Pressure Indicator Composite Films via Compressive Deformation of a Translucent Matrix Containing a Contrasting Filler., *ACS Appl. Mater. Interfaces*, 2024, **16**(15), 19432–19441.

